Unconventional enhancement of ferromagnetic interactions in Cd-doped $GdFe_2Zn_{20}$ single crystals studied by ESR and ^{57}Fe Mössbauer spectroscopies

M. Cabrera-Baez,[1,*] J. Munevar,[2,†] R. M. Couto-Mota,[1] Y. M. Camejo,[1] C. Contreras,[3] E. Baggio-Saitovitch,[3] M. A. Avila,[2] and C. Rettori[2,4]

[1]*Departamento de Física, Universidade Federal de Pernambuco, Recife, PE, 50740-560 Brazil*
[2]*CCNH, Universidade Federal do ABC (UFABC), Santo André, SP, 09210-580 Brazil*
[3]*Centro Brasileiro de Pesquisas Físicas, Rio de Janeiro, RJ, 2290-180 Brazil*
[4]*Instituto de Física "Gleb Wataghin," UNICAMP, Campinas, SP, 13083-859 Brazil*

(Received 24 July 2020; revised 20 September 2020; accepted 1 October 2020; published 14 October 2020)

Single crystals of $GdFe_2Zn_{20-x}Cd_x$ ($0.0 < x < 1.4$) were grown and characterized through structural, magnetic, and electronic properties using x-ray diffraction, field- and temperature-dependent magnetization, specific heat, ^{57}Fe Mössbauer spectroscopy, and electron spin resonance (ESR). A negative chemical pressure effect is accompanied by an unexpected increase of T_C from 86 to 96 K, together with a reduction of the magnetic effective moment and saturation magnetic moment, as evidenced by all of the experimental techniques. From the microscopic point of view, probing at the $4f$ electron level and the Fe nucleus has allowed the extraction of important information about the configuration and the effective role of the partial Cd substitution for Zn in this ferromagnetic system. Our ^{57}Fe Mössbauer spectroscopy experiments show a negligible variation of the hyperfine field at the Fe site, and ESR experiments reveal an enhancement of the Korringa-type relaxation and a molecular field effect as Cd is incorporated. This complex behavior is assigned to a possible reconstruction of the Fermi surface and/or a new distribution of the d type of conduction electrons in response to the negative chemical pressure, leading to an enhancement of the ferromagnetic transition temperature in a generalized Ruderman-Kittel-Kasuya-Yosida interaction scenario.

DOI: 10.1103/PhysRevB.102.144420

I. INTRODUCTION

Electronic correlations play a fundamental role in the development of new and interesting properties in materials, and are a central topic of study by experimental and theoretical scientists due to a variety of challenges emerging from quantum effects [1]. Canonical examples of materials with electronic correlation features are elemental Pt and Pd [2], known for their itinerant electrons collectively behaving as a system just below the border of the Stoner limit, which gives rise to a nearly ferromagnetic Fermi liquid (NFFL) [1]. Other, more complex systems were also found to feature NFFL properties, such as $TiBe_2$ [3], MCo_2 (M = Sc, Y, and Lu) [4], Ni_3Ga [5], and YFe_2Zn_{20} [6], presenting significant challenges toward their proper physical description.

Now, when $4f$ local moments are embedded in a system with NFFL features, rich phases emerge as a result of the interaction between $4f$ and d electrons, including the stabilization of a ferromagnetic (FM) ground state in some systems such as YCo_2 [7] and YFe_2Zn_{20} [6], when Y^{3+} ions are partially or fully replaced by rare-earth ions. Particularly, YFe_2Zn_{20} adopt a cubic $CeCr_2Al_{20}$-type structure with space group $Fd\bar{3}m$ (227), where the Y and Fe atoms occupy the $8a$ and $16d$ crystallographic sites, respectively, and the Zn atoms occupy three distinct sites ($96g$, $48f$, and $16c$) [8]. If Y^{3+} is replaced by Gd^{3+} ions (remaining in the same structure), the d type of electrons are polarized in the opposite direction by the Gd^{3+} moments, resulting in the stabilization of a remarkably high FM transition temperature of $T \approx 86$ K [6,9]. This scenario was further explored by Mössbauer experiments [10] which reported the absence of a hyperfine field on the ^{57}Fe site above $T \approx 90$ K, implying no clear evidence for the existence of such conduction electron polarization. However, another microscopic exploration using electron spin resonance (ESR) experiments in the concentrated system $GdFe_2Zn_{20}$ supported the idea of a polarized cloud of electrons, and proposed a "superexchangelike" mechanism to explain the emergence of this FM state [11].

Due to the electronic correlations, it is expected that tuning the system either by external pressure or by electron/hole doping can manipulate its FM response. This route was explored by Jia *et al.* [12], where a small substitution of Al for Zn ($GdFe_2Zn_{20-x}Al_x$) drastically reduces the FM ordering (from $T_C = 86$ K for $x = 0.0$ to $T_C = 10$ K for $x = 2.44$) as well as the itinerant electronic correlation, evidenced by the reduction of the Stoner coefficient from $Z = 0.88$ for $x = 0.0$ to $Z = 0.32$ for $x = 2.44$ in the case of crystals containing Y. These results provide insights on the role of band filling in the stabilization of FM interactions in a NFFL.

Another approach to explore this FM system is the dilution of the magnetic rare earth [13] as was the case of $Gd_xY_{1-x}Fe_2Zn_{20}$ for $0.0 < x < 1.0$, showing that FM order of the Gd^{3+} local moments persists down to $x = 0.02$, which is an exceptionally diluted case albeit strongly coupled to

*michael.cabrera@ufpe.br
†julian.munevar@ufabc.edu.br

 ©2020 American Physical Society

the d type of electrons from Fe. As a result of this $4f$-d coupling, a strong deviation from the high-temperature Curie-Weiss behavior upon approaching the ordering temperature was observed and the authors associate this behavior to an increasing coupling strength between Gd^{3+} and the highly polarizable electronic background of YFe_2Zn_{20} which have a strong temperature dependence following the s-d model [13].

Here, single crystals of $GdFe_2Zn_{20-x}Cd_x$ ($0 \leqslant x \leqslant 1.4$) were grown and characterized with the aim of inducing a "negative" pressure effect, in order to map possible changes in the system's magnetic ground state and to further exploring the aforementioned electronic interactions, as well as the deviation from Curie-Weiss (CW) behavior near to the transition in this FM compound, in a controlled manner. Such an approach was previously used in the closely related heavy-fermion system $YbFe_2Zn_{20}$, which showed strong suppression of the electronic hybridization in response to the same isoelectronic substitution, demonstrating an effective tool for tuning magnetic ground states in this family of compounds [14]. We show that inducing negative chemical pressure on $GdFe_2Zn_{20}$ leads to an unexpected enhancement of the FM transition temperature from $T_C = 83$ K for $x = 0.0$ to 94.5 K for $x = 1.4$, accompanied by a drastic reduction of the effective and saturation magnetic moments, evidencing an extreme sensitivity of the ground state to pressure. Additionally, the microscopic techniques of Mössbauer spectroscopy (to probe Fe sites) and ESR (using Gd as a local probe) were used in combination to elucidate these interesting properties and propose a new distribution of the d conduction electrons and/or a Fermi-surface reconstruction.

II. EXPERIMENTAL METHODS

Batches of $GdFe_2Zn_{20-x}Cd_x$ ($0 \leqslant x \leqslant 1.4$) single crystals were grown by the standard self-flux method [15,16] using excess of Zn. The constituent elements were 99.9% Gd, 99.9% Fe, 99.9999% Cd, and 99.9999% Zn (Alfa-Aesar). Initial ratios of elements were 1:2:47-y:y (y = 0–6) for the pseudoquaternaries Gd:Fe:Zn:Cd were weighted and sealed in an evacuated quartz ampoule and heated in a box furnace. Single crystals were grown by slowly cooling the melt between 1000 °C and 600 °C over 100 h. At 600 °C the ampoules were removed from the furnace, inverted, and placed in a centrifuge to spin off the excess flux following previous reports [9]. X-ray powder diffraction of crushed crystals were performed at room T to determine the crystal structures [8] and analyzed using a general structure analysis system (GSAS) [17] with the reported crystallographic data of $GdFe_2Zn_{20}$ as starting model [18] (Dataset ID sd_1226969). The effective Cd concentrations x for all of our samples were estimated using energy-dispersive x-ray spectroscopy (EDS) measurements in a JEOL-JSM-6010LA scanning electron microscope with a Vantage EDS system.

For the magnetic susceptibility ($\chi = M/H$) measurements, we used a Quantum Design MPMS3 superconducting quantum interference device (SQUID) magnetometer at various applied magnetic fields ($H \leqslant 6$ T) and temperatures (2.0 K $\leqslant T \leqslant 310$ K). The T-dependent specific heat (C_p) was measured in a Quantum Design Physical Properties Measurement System (PPMS) using the standard relaxation technique at zero field.

Temperature-dependent ^{57}Fe Mössbauer spectra were obtained at the Brazilian Center for Research in Physics (CBPF), Brazil, by recording the energy-dependent γ-ray transmission spectra on powdered specimens of the above-mentioned single crystals. A 14.4-keV γ-ray radiation source of ^{57}Co in a Rh matrix with about 50 mCi of activity, kept at room temperature, and a standard transmission spectrometer with sinusoidal velocity sweep were used. The temperature ranges for the Mössbauer spectra were from 3 to 120 K. For the ESR experiments, single crystals were crushed into fine powders of particle size greater than 100 μm, corresponding to an average grain size (d) larger than the skin depth (δ), $\lambda = d/\delta \gtrsim 10$. The X-Band ($\nu \approx 9.4$ GHz) ESR experiments were carried out in a conventional CW Bruker-ELEXSYS 500 ESR spectrometer using a TE_{102} cavity. The sample temperature was changed using a helium gas flux coupled to an Oxford T controller.

III. EXPERIMENTAL RESULTS

The following section is divided in two parts: macroscopic characterizations including XRD, specific heat, field- and temperature-dependent magnetization, and microscopic characterizations combining Mössbauer and ESR experiments.

A. Macroscopic characterizations

Figure 1 shows the (x-ray diffraction) XRD patterns of $GdFe_2Zn_{20-x}Cd_x$ ($0 \leqslant x \leqslant 1.4$). The refined lattice parameters $a = 14.121(9)$ Å for $GdFe_2Zn_{20}$ is in good agreement with the literature [9] and $a = 14.209(6)$ Å for $GdFe_2Zn_{18.6}Cd_{1.4}$ shows an expansion of the lattice due to Cd doping, preserving the same cubic phase. This expansion may also be observed in the Gd-Gd distance starting from 9.985(7) Å for $x = 0.0$ to 10.047(8) Å for $x = 1.4$ which will be useful in future discussions. Rietveld refinements of the $GdFe_2Zn_{20-x}Cd_x$ ($0 \leqslant x \leqslant 1.4$) structure allowing Cd atoms to partly occupy any of the three Zn sites converged to a solution where Cd prefers the 16c site (see Table I) in agreement with previous results [19]. Some peaks associated with Zn appear because the single crystals were obtained using Zn as a flux in the growth process and was difficult to remove from internal parts of the crystal affecting the χ^2 parameter.

It is worth mentioning that $Cd_{1.4}$ is in the limit of the Cd doping that $GdFe_2Zn_{20}$ admits by this single-crystal growth procedure, which is consistent with our findings and previous works [14] related to a strong preference of doping Cd atoms toward occupying exclusively the Zn3 crystallographic site in contrast with reported data of $GdFe_2Zn_{20-x}Al_x$ where Al appears to selectively occupy the Zn2 site [12]. This difference could be related to the important difference of the ionic radii of Al and Cd. To our knowledge, the ternary compound $GdFe_2Cd_{20}$ has not been reported yet.

Figure 2(a) shows C_P vs T for $GdFe_2Zn_{20-x}Cd_x$ ($0 \leqslant x \leqslant 1.4$). For $x = 0$ the FM transition at 83(1) K is in agreement with previously reported experiments [9], however, for $x = 1.4$ the FM transition increases, notably, to 95(1) K. The inset shows the increase of the FM transition temperature T_C as Cd

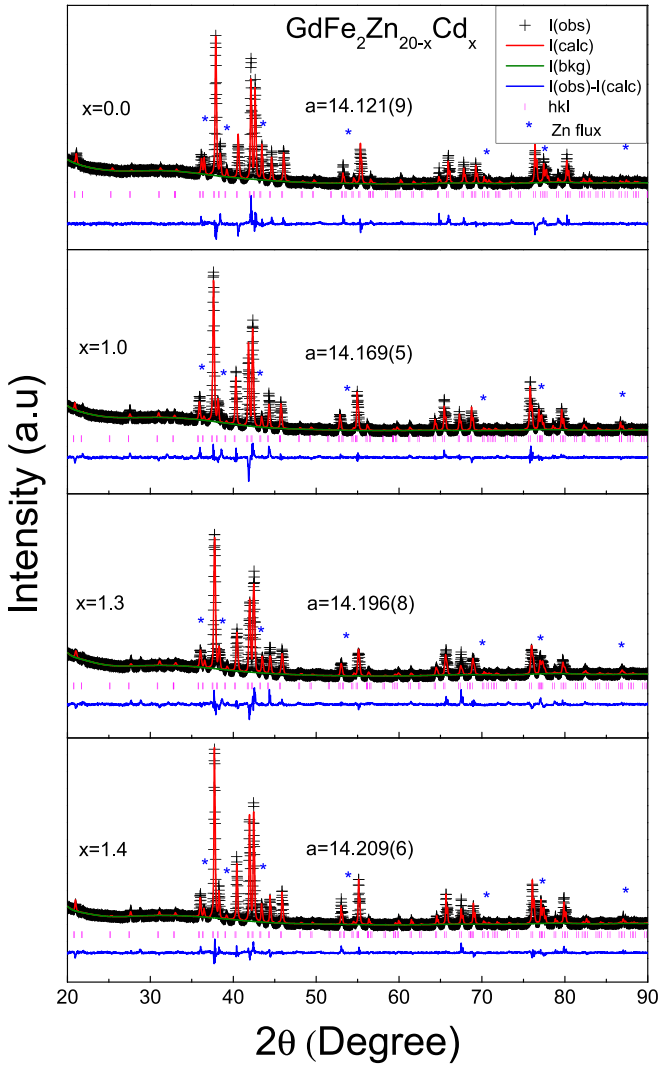

FIG. 1. Observed (black line with plus symbol), calculated (red line), background (green line), and difference (blue line) XRD profiles of $GdFe_2Zn_{20-x}Cd_x$ ($0 \leqslant x \leqslant 1.4$) recorded at room temperature. The Rietveld refinement was performed using GSAS. Asterisk denotes Zn flux.

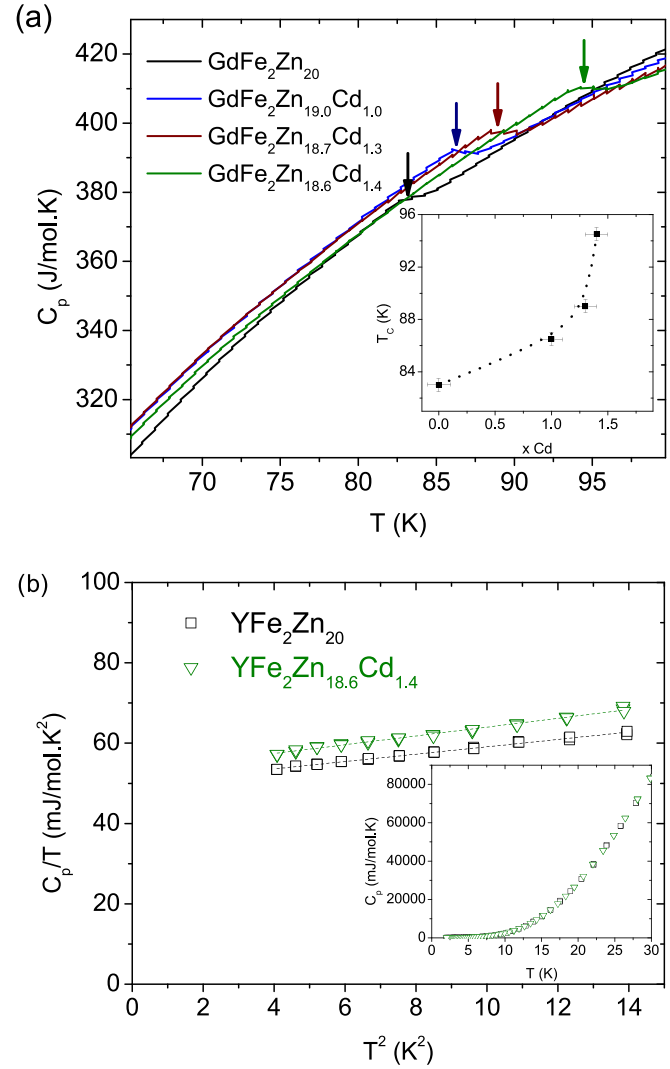

FIG. 2. (a) $C_P \times T$ for $GdFe_2Zn_{20-x}Cd_x$ ($0 \leqslant x \leqslant 1.4$) and (b) $C_P/T \times T^2$ for the reference system YFe_2Zn_{20} and $YFe_2Zn_{18.6}Cd_{1.4}$.

is incorporated in the system. Figure 2(b) shows C_P/T vs T^2 for the reference systems YFe_2Zn_{20} and $YFe_2Zn_{18.6}Cd_{1.4}$. The extrapolated Sommerfeld coefficients $\gamma = 52(1)$ mJ/mol K^2 and 54(1) mJ/mol K^2 for the pure and doped samples, respectively, and similar C_P vs T [see inset of Fig. 2(b)] are in good agreement with previous reported results in YFe_2Zn_{20} [6]. This result will be useful for our discussions in the following section.

TABLE I. Atomic coordinates and refined site occupancies from x-ray measurements for $x = 1.4$.

	x	y	z	Wyck	Occ
Gd	0.1250	0.1250	0.1250	8*a*	1.00
Fe	0.5000	0.5000	0.5000	16*d*	1.00
Zn1	0.0566	0.0566	0.3276	96*g*	1.00
Zn2	0.4930	0.1250	0.1250	48*f*	1.00
Zn3	0.0000	0.0000	0.0000	16*c*	0.79(8)
Cd	0.0000	0.0000	0.0000	16*c*	0.21(8)

Figure 3 presents T-dependent dc magnetic susceptibility. A typical FM transition is observed for the undoped compound $GdFe_2Zn_{20}$, in agreement with reported works [6,9,12,13]. Consistent with the above specific-heat results, it is also possible to see the effect of Cd substitution leading to the increase of the FM transition toward higher temperatures (83 K for $x = 0.0$ to 94.5 K for $x = 1.4$). A Curie-Weiss analysis, in the high-T region (200–310 K) of all our samples, indicates a remarkable change in the magnetic behavior, such as the reduction of the effective magnetic moment per formula unit μ_{eff} from 8.0 μ_B to 6.1 μ_B (inset of Fig. 3). Evaluation of the Curie-Weiss temperature for each sample indicates an increase from 60.2(8) K for the undoped sample to 64(2) K for $x = 1.4$ (Table II). The associated values of χ_0 related to the T-independent contribution to the dc magnetic susceptibility are summarized in Table II and will be discussed in the next section.

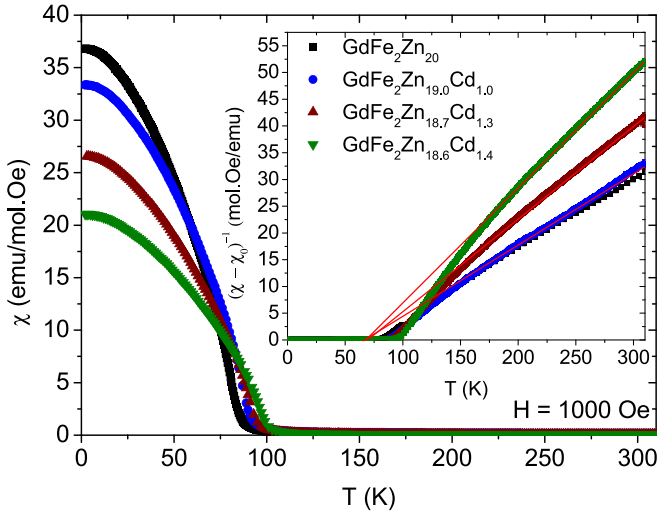

FIG. 3. dc magnetic susceptibility of $GdFe_2Zn_{20-x}Cd_x$ for $0.0 \leqslant x \leqslant 1.4$.

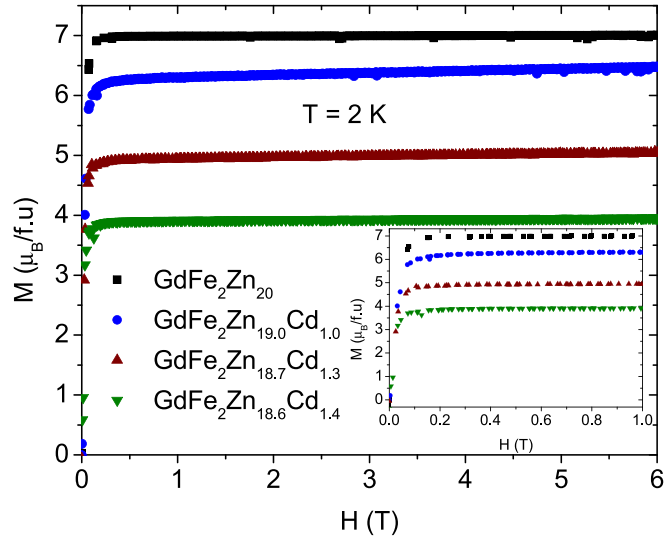

FIG. 4. Magnetization (M) vs magnetic field (H) at 2 K for $GdFe_2Zn_{20-x}Cd_x$ for $0.0 \leqslant x \leqslant 1.4$ and a zoom for low magnetic fields (inset).

Figure 4 shows the magnetization M vs H for $GdFe_2Zn_{20-x}Cd_x$ at 2 K. Once again, the dramatic effect of the Cd substitution at the Zn site is apparent, leading to a reduction of the saturation magnetic moment per formula unit $\mu_{\rm sat}$ from 6.9 μ_B/f.u. for the $x = 0$ sample to 4.0 μ_B/f.u. for $x = 1.4$, in agreement with the observed reduction of the effective magnetic moment (see Fig. 3).

The set of parameters found to describe the above macroscopic physical properties are summarized in Tables II and III for all our samples.

B. Microscopic characterizations: ^{57}Fe Mössbauer spectroscopy

Selected ^{57}Fe Mössbauer spectra obtained for the $x = 0$ and $x = 1.4$ crystals between 3 and 120 K are shown in Fig.5. The spectra at high T show a doublet that evolves to a broad spectrum composed by six superimposed lines at 3 K. This resonance doublet splitting is caused by a magnetic hyperfine field at the Fe site, reflecting the magnetic order already observed by the aforementioned techniques.

The obtained spectra were fitted within the Full Hamiltonian site model using the MOESSFIT software [20]. Three Fe sites were necessary to obtain a reasonable fit for all temperatures. The fitted hyperfine parameters are the isomer shift δ, the quadrupole splitting ΔE_Q, the magnetic hyperfine field B_{hf}, the angle θ between B_{hf}, and the main component of the electric field gradient V_{zz}, the spectral area A, and the linewidth Γ. We performed global fits for each sample, constraining the values of δ, ΔE_Q, θ, and B_{hf} for the sites 1 and 2, same Γ for all Fe sites, and the spectral areas for each site were set to be equal for all temperatures. According to Refs. [10,25], δ and the spectral area are expected to show T dependence, but we can safely assume these parameters as T independent because their variation within the temperature range we are performing in our analysis can be neglected. The fitted spectra above and below T_C for each sample are shown in Fig. 5.

From our fits (Fig. 5), we find that the ratio between the spectral areas of the main Fe sites is approximately 2:3, and the ratio of the third site to the main sites is 1:8. These sites successfully reproduce the experimental spectra throughout the whole T range studied. Below T_C, the corresponding angles θ for each site are 0°, 72(1)°, and 90°, which will be discussed in the following section. The linewidths extracted from our fits are 0.27(3) mm/s.

The fitted hyperfine parameters (δ, ΔE_Q, and B_{hf}) are shown in Fig. 6. From Fig. 6(a), δ for the main Fe sites is nearly T independent. However, it is seen that Cd doping causes a small increase in δ, a consequence of the variation in the s density of states at the Fe nucleus caused by the negative chemical pressure induced. The δ extracted from the third Fe site shows that the chemical environment is substantially different from the main phase, suggesting that Fe sites may be at sites with different local environment, such as the surface of the crystallites or sites with defects. The doping effect is also

TABLE II. Cd concentrations (x), FM transition temperature (from C_P) T_C, FM transition temperature (from χ) T_C, Curie-Weiss temperature $\Theta_{\rm CW}$, magnetic effective moment ($\mu_{\rm eff}$), magnetic moment of saturation ($\mu_{\rm sat}$), and the obtained value of χ_0 for the $GdFe_2Zn_{20-x}Cd_x$ system.

Conc. (x)	T_C (from C_P) (K)	T_C (from χ) (K)	$\Theta_{\rm CW}$ (K)	$\mu_{\rm eff}$ (μ_B/f.u.)	$\mu_{\rm sat}$ (μ_B/f.u.)	χ_0 (10^{-3} emu/mol Oe)
0.0	83.0(8)	82.5(7)	60.2(8)	8.0(1)	6.9(1)	4.0(1)
1.0	86.5(8)	87.5(6)	62(2)	8.0(1)	6.5(1)	12.0(1)
1.3	89.0(8)	90.0(6)	64.0(8)	7.7(1)	5.0(1)	43.0(1)
1.4	94.5(8)	95.5(7)	64(2)	6.1(1)	4.0(1)	21.0(1)

TABLE III. Structural lattice parameters obtained from the Rietlveld refinement for $GdFe_2Zn_{20-x}Cd_x$ ($0 \leqslant x \leqslant 1.4$).

Sample	$GdFe_2Zn_{20}$	$GdFe_2Zn_{19.0}Cd_{1.0}$	$GdFe_2Zn_{18.7}Cd_{1.3}$	$GdFe_2Zn_{18.6}Cd_{1.4}$
a (Å)	14.121(9)	14.169(5)	14.196(8)	14.209(6)
V (Å^3)	2816.(3)	2844.(8)	2861.(3)	2869.(1)
ρ (g/cm^2)	7.436	7.428	7.404	7.391
χ^2	6.643	4.358	6.300	6.411
wRp(%)	4.47	3.58	4.60	4.64
Rp(%)	2.91	2.55	3.14	2.99
Gd-Gd (Å)	9.985(7)	10.019(4)	10.038(7)	10.047(8)
Gd-Fe (Å)	5.854(6)	5.874(4)	5.885(9)	5.891(0)

seen in ΔE_Q [Fig. 6(b)], where a reduction is observed for the sample with $x = 1.4$.

The T dependence of B_{hf} shown in Fig. 6(c) reflects the onset of the magnetic order for each studied sample. From Figs. 5 and 6(c) it is seen that there is no magnetic hyperfine field at the Fe site above T_C, suggesting that the moment correlations observed above T_C either have origin in another magnetic element or that the magnetic correlations lie below the Mössbauer spectroscopy detection limit. Finally, the resonance linewidth Γ [Fig. 6(d)] is reflecting similar behavior for both specimens, suggesting that the doping is not causing a considerable line broadening.

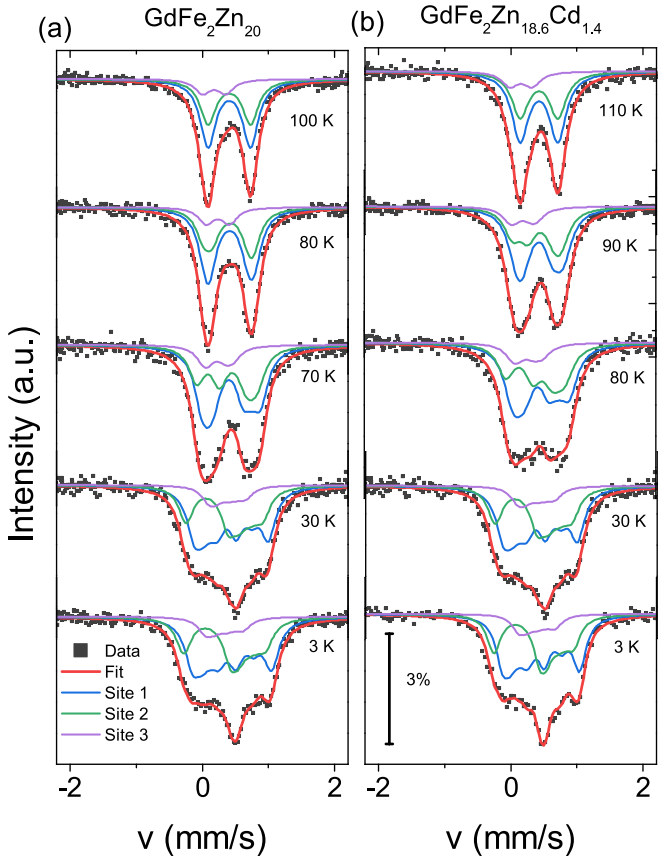

FIG. 5. Temperature-dependent ^{57}Fe Mössbauer spectra for $GdFe_2Zn_{20-x}Cd_x$ with (a) $x = 0$ and (b) $x = 1.4$. In addition, the Fe sites employed for the fits are shown above and below T_C.

C. Microscopic characterizations: ESR

In order to further investigate the peculiar increase of the FM transition temperature due to the Cd substitution, we use T-dependent ESR to elucidate the strength of the short-range interaction just above the FM transition temperature.

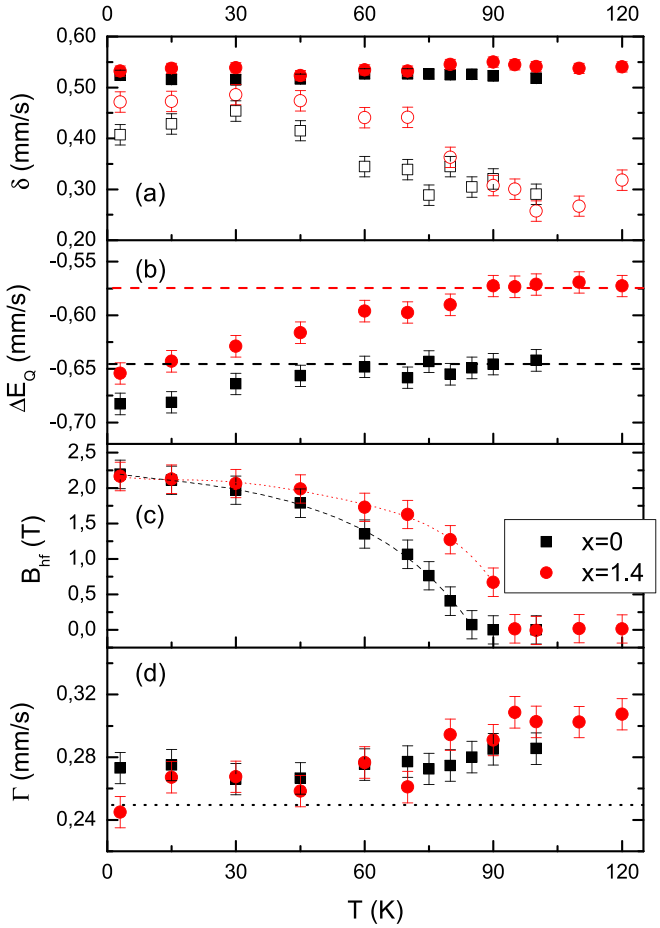

FIG. 6. ^{57}Fe Mössbauer hyperfine parameters for $GdFe_2Zn_{20-x}Cd_x$: (a) Chemical isomer shift δ for the main and the so-called impurity phases, (b) electric quadrupole splitting ΔE_Q (dotted lines represent the values at low temperatures above T_C), and (c) magnetic hyperfine field at the Fe site B_{hf} and their respective fitting curves, and (d) the resonance linewidth Γ (dotted lines represent the values found for the nonmagnetic specimens $LuFe_2Zn_{20}$ and $YbFe_2Zn_{20}$ [10]).

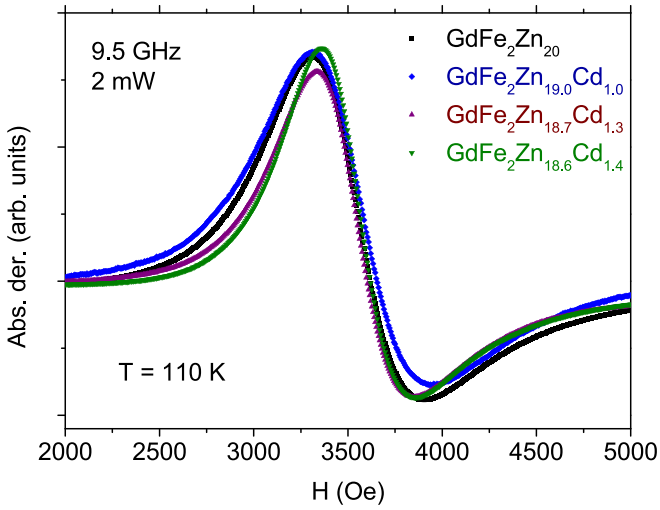

FIG. 7. ESR of Gd^{3+} at 9.5 GHz, 2 μW at $T = 110$ K for $GdFe_2Zn_{20-x}Cd_x$ ($0.0 \leqslant x \leqslant 1.4$).

Figure 7 shows the ESR of Gd^{3+} at 9.5 GHz frequency, 2 μW power, and $T = 110$ K for $GdFe_2Zn_{20-x}Cd_x$ ($0.0 \leqslant x \leqslant 1.4$). The obtained spectra for all samples show the typical Dysonian line shape expected for metallic systems, with a small detectable change in the linewidth but similar resonance fields for all of the studied samples.

Figure 8 shows the T evolution of the Gd^{3+} ESR linewidth ΔH for all our samples. The linear behavior $\Delta H = a + bT$, where a is the residual linewidth ΔH_0 and $b = \frac{dH}{dT}$ the thermal broadening of the linewidth (Korringa rate) [21] associated to the exchange interaction between the Gd^{3+} $4f$-localized magnetic moment and the conduction electrons (ce), J_{fce}. The experiments show an increase of the Korringa rate from $b = 14.0$ Oe/K for the pure sample to $b = 20.0$ Oe/K for $x = 1.4$. At temperatures close to T_C the linear behavior ceases for each Cd concentration due to the Gd-Gd magnetic interactions, in agreement with the dc magnetic susceptibility measurements.

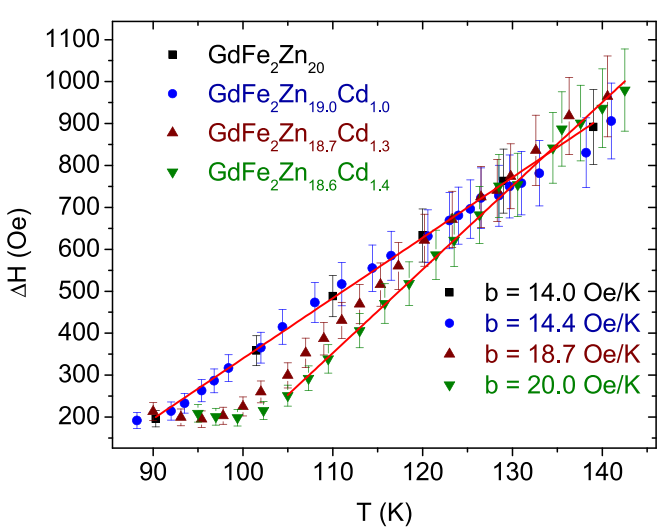

FIG. 8. T-dependent Gd^{3+} ESR linewidth ΔH for $GdFe_2Zn_{20-x}Cd_x$ ($0.0 \leqslant x \leqslant 1.4$).

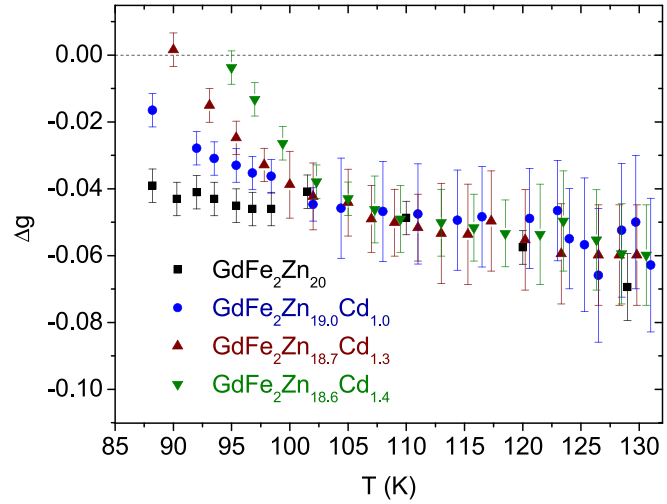

FIG. 9. g shift (Δg) for $GdFe_2Zn_{20-x}Cd_x$ for $0.0 \leqslant x \leqslant 1.4$.

Other temperature-dependent differences are manifested in the resonance field (H_{res}), related to the g factor by the resonance condition $h\nu = g\mu_B H_{res}$, where ν is the frequency, h the Planck constant, and μ_B the Bohr magneton. This g factor can be compared with the value obtained from Gd^{3+} in insulators, $g = 1.993$, yielding a g shift caused by the local polarization of the conduction electrons.

Figure 9 presents the T dependence of the Gd^{3+} ESR g shift, $\Delta g = g - 1.993$. At $T \gtrsim 100$ K, Δg is negative [$\approx -0.06(1)$)] for all of our samples, with a weak T dependence consistent with our previous work [11]. Notice that, within the range of 110 K $\lesssim T \lesssim$ 130 K where there is a deviation of the dc magnetic susceptibility from the high-T Curie-Weiss behavior (inset Fig. 3), the measured Δg for all our samples present the same value of $\Delta g = -0.06(1)$. However, within the interval of 90 K $\lesssim T \lesssim$ 107 K and for the Cd-doped samples, there is a clear decrease in magnitude of the negative-g shift, assigned to the emergence of short-range FM magnetic interactions in the Cd-doped samples (see Fig. 3).

IV. ANALYSIS AND DISCUSSION

The expected lattice expansion due to the Cd substitution has been confirmed by the increase of the lattice parameter, from $a = 14.121(9)$ Å for $GdFe_2Zn_{20}$ to $a = 14.209(6)$ Å for $GdFe_2Zn_{18.6}Cd_{1.4}$. This results in a "negative" chemical pressure as a consequence of the larger ionic radius of Cd compared to Zn (Fig. 1). However, as the Gd-Gd separation increases (Table III) with x, our C_P vs T (Fig. 2) results evolve in the opposite way of the conventional expectation, showing an *increase* of T_C from 83 K for $x = 0$ to 95 K for $x = 1.4$. Previous experiments in this FM system under hydrostatic pressure up to 7 kbar [9] revealed a small reduction of T_C with $\frac{dT_C}{dP} = -0.17(1)$ K/kbar, and this reduction was explained in terms of the variation of the lattice parameter yielding no steric effects in the suppression of the T_C. "Positive" chemical pressure with electron doping was also studied through Al substitution at the Zn site [12], wherein a reduction of the electronic correlation and a strong decrease of T_C was observed. Although important results were obtained, the individual roles

of pressure and electron doping were not resolved, which is necessary for the comprehension of those effects. The present results obtained from XRD and C_P demonstrate that small changes in the composition made by isoelectronic substitution of Zn for Cd have induced significant changes in the magnetic properties. The unexpected increase of T_C has led the $x = 1.4$ sample to reach the highest FM transition temperature ($T_C \sim$ 100 K) among both the RT_2Zn_{20} family (R = Gd-Tm [22]) and the RT_2Cd_{20} family (R = rare earth, T = Ni, Pd) [23]. Figure 3 confirms the enhancement of the FM transition temperature T_C from 82.5(7) K for $x = 0.0$ to 95.5(7) K for $x = 1.4$, consistent with the FM bulk transition revealed from Fig. 2. Hence, Cd effects in this FM system deserve thorough investigation.

The Curie-Weiss temperatures Θ_{CW} were also derived (Table II), yielding an increase from 60.2(8) K for $x = 0$ to 64(2) K for $x = 1.4$. There is a fundamental difference between the variation of T_C ($\Delta T_C = 11.5$ K) and Θ_{CW} ($\Delta\Theta_{CW} = 3.8$ K) for $x = 0$ and 1.4 that comes from the deviation of the linear behavior above 200 K for all studied samples [Fig. 3(b)]. This deviation is justified as a polarization of the d-type conduction electrons (electronic cloud) in the opposite direction of Gd^{3+} near the FM transition [6], which therefore directly affects T_C, but not Θ_{CW} obtained from high-temperature extrapolation. The reason behind the observed changes may be a drastic modification of the itinerant molecular field, responsible for the CW deviation. Figure 3(b) and Table II also evidence an increasing slope of the linear fitting to the inverse dc magnetic susceptibility, based on the CW formalism, resulting in decrease of the estimated magnetic effective moment from $\mu_{\rm eff} = 8.0(1)\,\mu_B$/f.u. for $x = 0$ (expected for Gd^{3+} from Hund's rules) to $\mu_{\rm eff} = 6.1(1)\,\mu_B$/f.u. for $x = 1.4$. This reduction indicates the emergence of a strong contribution opposite to the Gd^{3+} moments but still persistent at high temperatures, which is in principle unexpected from the inclusion of filled-shell Cd atoms without any magnetic moment. This scenario reinforces the assumption of a strong modification of the itinerant molecular field with negative chemical pressure oriented in opposition to the Gd^{3+} magnetic moments giving an extra contribution to the CW behavior.

It is worth mentioning that despite the reduced range of the linear fitting of $(\chi\text{-}\chi_0)^{-1}$ in the pure sample (for $x = 0$), the obtained values of $\mu_{\rm eff}$ and $\mu_{\rm sat}$ are in very good agreement with expected values using the Hund's rules. This gives us confidence to use it as a reference for the Cd-doped samples, where is expected a complex behavior. The T-independent term of the dc magnetic susceptibility (see Table III) comes from Pauli paramagnetism (with electronic correlations), cage diamagnetism, atomic diamagnetism (sample + Zn impurities), and the sample holder (already subtracted in our data). The Cd ions could modify (in some quantitative degree, unknown for us) those dependent/independent contributions, affecting the χ_0 (not systematic in agreement with Table II). Although the Curie-Weiss analysis was used in a safe range of temperatures, it is possible to have an extra influence in the obtained values for $\mu_{\rm eff}$ in Cd-doped samples, dependent of the χ_0 value. We believe that comprehensive studies using single crystals of $YFe_2Zn_{20-m}Cd_m$ will be necessary to clarify this issue. These χ_0 modifications will be a subject of a future detailed report.

Consistent with the above hypothesis but now at low temperatures, Fig. 4 shows a strong reduction of the magnetic saturation moment from $\mu_{\rm sat} = 6.9(1)\,\mu_B$/f.u. for $x = 0$ to $\mu_{\rm sat} = 4.0(1)\,\mu_B$/f.u. for $x = 1.4$. It is worth noting that the calculated Rhodes-Wohlfarth ratios ($\frac{\mu_{\rm eff}}{\mu_{\rm sat}}$) of 1.14 for $x = 0$ and 1.53 for the threshold $x = 1.4$ validate a localized magnetic moment description for all measured samples but leaves an open scenario of a possible small coexistence with emergent itinerant magnetic moments when Cd is in the system.

An extra contribution to the magnetism for this FM compound was proposed from XRMS, XMCD, and XANES experiments by Mardegan *et al.* [24], where Gd^{3+} ions induce a small magnetic moment in the $4p$ states due to the short Gd-Zn distances, leading to another possible interpretation of the observed results in this work. In order to probe those effects locally and elucidate the correct mechanism involved, it is necessary to explore the system by microscopic techniques.

We have used the Fe nucleus as a probe below the FM transition by ^{57}Fe Mössbauer spectroscopy. In particular, we observe the interaction of the d electrons associated to the Fe atom and their local surroundings. Fits of our spectra using one Fe site [10] and two Fe sites with a fixed spectral area ratio of 1:3 [25] were tested, but neither model gave satisfactory fits. Our analysis gave a spectral area ratio of 2:3 for the main sites, which could be explained if we consider the direction of V_{zz} along the [111] axis, taking into account that the Gd atoms themselves form a corrugated honeycomb lattice and the Fe atoms form a pyrochlore lattice. In this case, $\frac{1}{3}$ of the Fe atoms are sensing the transferred FM field from the Gd moments pointing along the [111] direction ($\theta = 0^\circ$), and the remaining $\frac{2}{3}$ of the Fe sites correspond to the Gd moments pointing off the [111] axis ($\theta = 72^\circ$).

The quadrupole splitting ΔE_Q above T_C varies upon doping from $-0.64(2)$ mm/s ($x = 0$) to $-0.57(2)$ mm/s ($x = 1.4$). Since we are dealing with metallic crystals, the conduction electrons involved in the V_{zz} are not necessarily bound to an atom and cannot be categorized strictly as external or local. In this case, V_{zz} can be simplified to [26]

$$V_{zz} = V_{zz}^c - K(1 - \gamma_\infty)V_{zz}^{\rm latt}, \tag{1}$$

where V_{zz}^c is the main component of the electric field gradient (EFG) for local electrons belonging to impurities or additional contributions, K is an empirical factor accounting for the nature of the EFG due to conduction electrons, γ_∞ is the corresponding antishielding factor, and $V_{zz}^{\rm latt}$ is the contribution to the EFG from the crystal lattice. The K constant varies between 1 and 2 depending on the strength of V_{zz}. We performed lattice sums of $V_{zz}^{\rm latt}$ just by calculating the contribution of each atom in the unit cell, obtaining the V_{ij} elements of the EFG tensor and performing numerical diagonalization of the matrix to obtain $V_{zz}^{\rm latt}$. Afterward, we take $K = 1$ in Eq. (1) (see Ref. [26]) to obtain V_{zz}. To obtain ΔE_Q^{calc} we use the following expression:

$$\Delta E_Q^{\rm calc} = \frac{e^2 Q V_{zz}}{2}, \tag{2}$$

where e is the electron charge and Q is the quadrupole moment of the Fe nucleus in its excited spin state $I = \frac{3}{2}$ ($Q =$ 160 mbarn). We obtained $\Delta E_Q^{\rm calc} = -0.61$ mm/s for $x = 0$

and $\Delta E_Q^{\text{calc}} = -0.56$ mm/s for $x = 1.4$. By comparing these calculations with the experimental values of ΔE_Q, we notice that the calculated values are very close to the experimental values, meaning that the effect of impurities via a hypothetical V_{zz}^c can be neglected, and confirming the isoelectronic Cd doping in $GdFe_2Zn_{20}$. Furthermore, the tendency toward an isotropic Fe local environment by Cd doping, seen previously as a decrease of ΔE_Q for increasing a lattice parameters, is also confirmed [10].

Another interesting feature observed from Fig. 6(b) is that below T_C is observed a further decrease of ΔE_Q. This can be explained by considering that any dipolar field acting at the Fe nucleus is proportional to the electronic contribution to V_{zz}, or $B_D = \mu_B q$, where μ_B is the Bohr magneton and q is the electronic contribution to V_{zz}. This is an indication of the presence of a transferred hyperfine field from the Gd moments to the Fe nucleus, which will be considered below.

Figure 6(c) shows the temperature dependence of B_{hf} extracted from the fits. We fitted the B_{hf} with the function

$$B_{hf}(T) = B_{hf}(0)\left[1 - \left(\frac{T}{T_C}\right)^{\alpha}\right]^{\beta}, \tag{3}$$

where $B_{hf}(0)$ is the value of the hyperfine field at absolute zero temperature, T_C is the magnetic transition temperature, and α and β are exponents that are associated with the behavior of B_{hf} at temperatures close to 0 and T_C, respectively. The values of the above-mentioned parameters for the $x = 0$ sample are $B_{hf}(0) = 2.19(3)$ T, $T_C = 81.6(7)$ K, $\alpha = 1.7(2)$, and $\beta = 0.50(6)$; whereas for the $x = 1.4$ sample we get $B_{hf}(0) = 2.16(3)$ T, $T_C = 91.8(9)$ K, $\alpha = 2.0(4)$, and $\beta = 0.36(6)$.

From these results, T_C increases with Cd doping, in agreement with our C_P and magnetization results. The different α and β obtained from the fits suggest a tendency to different mechanism for the magnetic order in the doped sample. The deviation of α from the expected value within the Bloch's $\frac{3}{2}$ law as doping increases can be related to different magnetic excitation mechanisms, whereas the decrease of β can be associated with the change in the critical behavior of the magnetic state induced by Cd doping. This can be caused by preformed internal fields above T_C, responsible for the deviation of χ^{-1} from the Curie-Weiss law above T_C. These preformed internal fields, whose origin may be the polarization of the electronic cloud, may be below the Mössbauer spectroscopy sensitivity to small hyperfine fields. However, it can be seen in Fig. 6(d) that Γ decreases below T_C to values close to those reported for nonmagnetic $LuFe_2Zn_{20}$ in Ref. [10] ($\sim$0.25 mm/s), and this decrease could be explained by a correct estimation of the total hyperfine field at lower temperatures, including the contribution of this electronic cloud polarization field seen above T_C.

The nature of $B_{hf}(0)$ can be elucidated by considering the main contributions to B_{hf}, namely, dipolar fields B_D and from the Fermi contact field B_C, the latter composed by a core polarization term and a conduction band polarization term ($B_C = B_{cp} + B_{\text{cep}}$). We estimate that $B_D \sim 0.5$ T for $GdFe_2Zn_{20}$, and the corresponding difference ($B_C = B_{hf} - B_D \simeq 1.7$ T) can be associated to intrinsic, itinerant Fe moments, whose magnetic moments per Fe atom should be between 0.11 μ_B and 0.2 μ_B. We consider that the equivalence between μ_{Fe} and B_{hf} should be between 10.4 T/μ_B15.2 and T/μ_B. A similar result was inferred from Mössbauer spectra of $DyFe_2Zn_{20}$ [25]. Ideally, the increase of T_C should be related to an increase in B_{hf}. Thus, the absence of such correlation in our results could be partially explained by a compensation of the increase of the core polarization hyperfine field B_{cp} (bound to Fe) by an increasing band polarization hyperfine field B_{cep} (doping effect), which may be coming from the redistribution of the polarized d type of ce at the Fermi surface. These two effects overlap leading to a negligible variation of $B_{hf}(0)$ but with an increase in T_C, and since B_{cp} and B_{cep} are both changing, the overall behavior is expected to change, affecting α and β. This hypothesis will be confirmed below with our ESR results.

At this point, it is clear that the effects of Cd doping on the FM system $GdFe_2Zn_{20}$ are to increase the Gd-Gd separation, to increase the FM transition temperature, and to decrease the magnetic effective and saturation moment, with a possible itinerant local field modification. We thus turn to the analysis of the ESR results for $T \gtrsim 105$ K, i.e., in the paramagnetic region. Figure 8 shows an increase in the thermal broadening of the ESR linewidth (Korringa rate) from $b = 14.0$ Oe/K to $b = 20.0$ Oe/K as the Cd concentration increases from $x = 0$ to 1.4, whereas the g shift (Fig. 9) remains about the same with a value of $\Delta g \approx -0.06$. This is an indication that there is no bottleneck nor dynamic effects in this system [27]. In a single d-band ce model for $GdFe_2Zn_{20-x}Cd_x$ and for an exchange interaction $J_{fd}(0)\vec{S}_f \cdot \vec{s}_d$, [in the absence of ce momentum transfer [28], $q = 0$, i.e., $\langle J_{f.d}(q)\rangle_F = J_{f.d}(0)$], between the localized $4f$-electron spins of Gd^{3+}, $\vec{S}_f$, and those of the ce, $\vec{s}_d$, the g shift. and the Korringa rate b are correlated as follows [29]:

$$\Delta g = J_{fd}(0)\eta_F \tag{4}$$

and

$$b = \frac{d(\Delta H)}{dT} = \frac{\pi k_B}{g\mu_B} J_{fd}^2(0)\eta_F^2 = \frac{\pi k_B}{g\mu_B}(\Delta g)^2, \tag{5}$$

where η_F is the "bare" density of states at the Fermi surface, k_B is the Boltzmann constant, μ_B is the Bohr magneton, and g is the Gd^{3+} g value. Then, as $\pi k_B/g\mu_B = 2.34 \times 10^4$ Oe/K, for a g shift of $\Delta g \approx -0.06$ one may expect a Korringa rate of about 85 Oe/K using Eq. (2), which is much larger than the maximum measured value of $b = 20.0$ Oe/K for $x = 1.4$. Since there is only a 4% change in the Sommerfeld coefficient with the Cd doping [see Fig. 2(b)], there should be no considerable change in the density of states η_F at the Fermi level and therefore a strong q dependence of the exchange interaction $J_{fs}(q)$ is evident in this system. Hence, as the Cd concentration increases, there should be a concomitant increase of the average of the exchange interaction over the Fermi surface $\langle J_{fd}(q)\rangle_F$. Then, for an exchange interaction that depends on the ce momentum transfer q and electronic correlations the above equations read as

$$\Delta g = \frac{J_{fd}(0)\eta_{Fd}}{1 - \alpha_d} \tag{6}$$

and

$$b = \frac{\pi k_B}{g\mu_B}\left[F_d \frac{\langle J_{fd}^2(q)\rangle_F \eta_{Fd}^2}{(1-\alpha_d)^2} K(\alpha_d)\right], \tag{7}$$

where α_d is the Stoner parameter, $K(\alpha_d)$ the reduction factors of the Korringa relaxation for core polarization [30,31], and $F_d = \frac{1}{5}$ factor associated with the orbital degeneracy of the unsplit (no crystal-field effects) bands at the Fermi level. Thus, using the Sommerfeld coefficient γ from Fig. 2(b) [$\eta_{Fd} = 3.05(1)$ states eV/f.u. in agreement with density functional theory calculations [11]], the experimental values for the g shift (-0.06), the Korringa rates b (14 Oe/K for $x = 0$ and 20 Oe/K for $x = 1.4$), $\alpha = 0.51$, $K(\alpha) = 0.6063$ [11,30,31] (assuming similar correlation parameters in the analysis [30]) for $GdFe_2Zn_{20}$ in Eqs. (3) and (4) we estimate $J_{fd}(0) = -20(6)$ meV (for $x = 0.0$ and 1.4) and $\langle J_{fd}(q)\rangle_F = 11.4(6)$ meV for $x = 0$ and 13.4(7) meV for $x = 1.4$. These results lead us to conclude that the lattice expansion by the Cd doping does not change the d-ce polarization at the Gd^{3+} ions but enhances the ce spin-flip scattering on the Fermi surface. This enhancement is associated to a modification of the Fermi surface and/or to a redistribution of the ce on the Fermi surface. A redistribution of d-ce may be the origin for the unexpected increase of the FM transition temperature T_C and also for short-range FM correlations above ≈100 K that deviate the susceptibility from the high-T CW behavior (inset Fig. 3). It is worth mentioning that our ESR result could be reasonably well described within a single-band d-ce model. Therefore, these results do not support the suggestion put forward by Mardegan *et al.* [24] that Zn 4p-ce may be also participating at the Fermi surface, which would manifest in our results as a multiband case giving Cd concentration dependence of the g shift in the paramagnetic region [28].

Figure 9 shows that for 85 K $\lesssim T \lesssim$ 105 K there is an evident T dependence of the g shift in consequence of long-range set-in FM correlations that give rise to a Cd concentration dependent internal local FM magnetic field at the Gd^{3+} sites. With this and near to the FM transition, the measured g of each sample must be understood as an "effective" value (g_{eff}) with the T dependence related to an internal molecular field as $g_{\text{eff}} = g[1 \pm \lambda_x \chi]$ [32,33], where χ is the $GdFe_2Zn_{20-x}Cd_x$ ($0.0 \leqslant x \leqslant 1.4$) magnetic susceptibility for 85 K $\lesssim T \lesssim$ 105 K and λ_x the associated molecular field constant for each x.

This approach is very well supported by the strong similarities in the temperature dependence of these two independent measurements, such as the g shift and the dc magnetic susceptibility, shown in Fig. 10(a) for 85 K $\lesssim T \lesssim$ 110 K. Nonetheless, the obtained values have to be taken with care in view of the different magnetic field applied in each technique leading just a rough estimation of the molecular field constant λ.

In a real material, the internal magnetic field ($\vec{H}_{\text{int}}$) is related to the magnetization ($\vec{M}$) and to the external magnetic field ($\vec{H}_{\text{ext}}$) as $\vec{H}_{\text{int}} = \vec{H}_{\text{ext}} \pm \lambda\vec{M}$, where λ is the molecular field constant [34]. This λ is also related to the FM transition temperature as $T_C = \lambda C$, where C is the Curie constant.

Remembering the resonance condition $h\nu = g\mu_B H_{\text{res}}$ mentioned above and based on Fig. 10(a), it is possible to infer the behavior of the internal molecular field with the Cd concentration x near to the FM transition. With this and taking the modulus, it is possible to plot $H_{\text{int}} = H_{\text{res}}(\text{low } T)$-$H_{\text{res}}(\text{high } T)$) as a function of the associated magnetization (M) at the same temperature as shown in Fig. 10(b). The

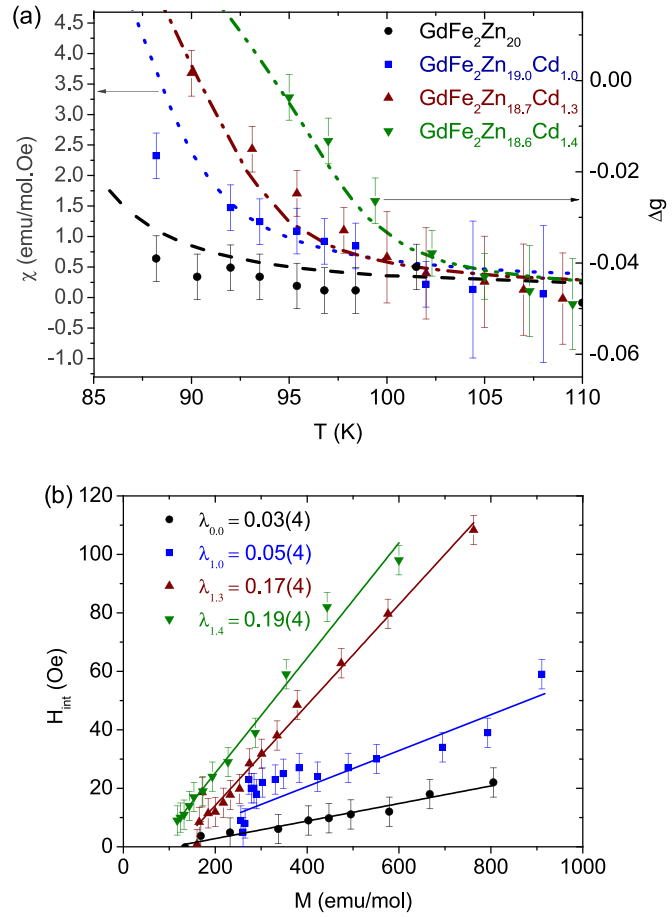

FIG. 10. (a) Comparison of the temperature dependence of the dc magnetic susceptibility and effective g shift for $GdFe_2Zn_{20-x}Cd_x$ for $0.0 \leqslant x \leqslant 1.4$ near to their respective FM transition and (b) internal magnetic field [$H_{\text{int}} = H_{\text{res}}(\text{low } T)$-$H_{\text{res}}(\text{high } T)$ vs magnetization (M) evaluated at the same temperature.

estimated molecular field constants λ_x for each x reveals an increment from $\lambda_{0.0} = 0.03(4)$ mol Oe/emu to $\lambda_{1.4} = 0.19(4)$ mol Oe/emu consistent with the obtained increment in the FM transition temperature when Cd is added despite the observed reduction of the Curie constant related to the effective magnetic moment μ_{eff}. Due to the difference in the magnetic field strength in each technique, those extracted molecular field constants must be renormalized by a factor of $\frac{1}{3}$ since the resonance field is near to 3000 Oe and the magnetic field used in dc susceptibility measurements was 1000 Oe. Thus, it was possible to associate the enhancement of the FM transition temperature to the modification of the itinerant molecular field of d type of conduction electrons from Fe. This modification also leads to a reduction of μ_{eff} and μ_{sat} in view of an antiparallel cloud of d-type conduction electrons present above and below the FM transition temperature as was explored by two different spectroscopic techniques.

V. CONCLUSIONS

Single crystals of the $GdFe_2Zn_{20-x}Cd_x$ were successfully grown for $0.0 < x < 1.4$ and characterized by XRD,

magnetization, heat capacity, ESR, and Mössbauer. The small, isoelectronic Cd inclusion in the lattice was found to produce drastic and unexpected effects, leading to an enhancement of the ferromagnetic Gd-Gd interaction while reducing the effective magnetic moment and saturation moment. ESR and Mössbauer experiments confirm the unconventional form of ferromagnetic ordering in the pure and doped system, and a redistribution of the polarized d type of ce/Fermi-surface modification, proposed to be responsible for the FM ordering in doped samples. This effect has led to the doped sample with $x = 1.4$ achieving the highest FM transition temperature among the RT_2X_{20} families ($R =$ rare earth, $T =$ transition metal), $X =$ Zn, Cd).

ACKNOWLEDGMENTS

This work was supported by Brazilian agencies CNPq, CAPES, FINEP and FAPESP (Grants No. 2017/10581-1 and No. 2011/19924-2). We are thankful to the UFABC CEM for providing access to its experimental facilities.

[1] T. Moriya, *Spin Fluctuations in Itinerant Electron Magnetism* (Springer, Berlin, 1985).
[2] B. Zellermann, A. Paintner, and J. Voitlander, J. Phys. Condens. Matter **16**, 919 (2004).
[3] B. T. Matthias, A. L. Giorgi, V. O. Struebing, and J. L. Smith, Phys. Lett. **69**, 221 (1978).
[4] R. Lemaire, Cobalt (Engl. Ed.) **33**, 201 (1966).
[5] F. R. de Boer, C. J. Schinkel, and J. Biesterbos, Phys. Lett. **25**, 606 (1967).
[6] S. Jia, S. L. Budko, G. D. Samolyuk, and P. C. Canfield, Nat. Phys. **3**, 334 (2007).
[7] T. Tsuchida, S. Sugaki, and Y. Nakamura, J. Phys. Soc. Jpn. **39**, 340 (1975).
[8] T. Nasch, W. Jeitschko, and U. C. Rodewald, Z. Naturforsch. B **52**, 1023 (1997).
[9] S. Jia, N. Ni, G. D. Samolyuk, A. Safa-Sefat, K. Dennis, H. Ko, G. J. Miller, S. L. Bud'ko, and P. C. Canfield, Phys. Rev. B **77**, 104408 (2008).
[10] S. L. Bud'ko, Tai Kong, X. Ma, and P. C. Canfield, J. Phys.: Condens. Matter **27**, 336003 (2015).
[11] M. Cabrera-Baez, A. Naranjo-Uribe, J. M. Osorio-Guillén, C. Rettori, and M. A. Avila, Phys. Rev. B **95**, 104407 (2017).
[12] N. Ni, S. Jia, G. D. Samolyuk, A. Kracher, A. S. Sefat, S. L. Bud'ko, and P. C. Canfield, Phys. Rev. B **83**, 054416 (2011).
[13] S. Jia, N. Ni, S. L. Bud'ko, and P. C. Canfield, Phys. Rev. B **76**, 184410 (2007).
[14] M. Cabrera-Baez, R. A. Ribeiro, and M. A. Avila, J. Phys.: Condens. Matter **28**, 375601 (2016).
[15] P. C. Canfield and Z. Fisk, Philos. Mag. **65**, 1117 (1992).
[16] R. A. Ribeiro and M. A. Avila, Philos. Mag. **92**, 2492 (2012).
[17] B. H. Toby and R. B. Von Dreele, J. Appl. Crystallogr. **46**, 544 (2013).
[18] P. Villars and K. Cenzual, *Inorganic Solid Phases* (Springer, Heidelberg, 2012).
[19] K. Wakiya, T. Onimaru, S. Tsutsui, T. Hasegawa, K. T. Matsumoto, N. Nagasawa, A. Q. R. Baron, N. Ogita, M. Udagawa, and T. Takabatake, Phys. Rev. B **93**, 064105 (2016).
[20] S. Kamusella and H. H. Klauss, Hyperfine Interact. **237**, 82 (2016).
[21] J. Korringa, Physica (Amsterdam) **16**, 601 (1950).
[22] S. Jia, N. Ni, S. L. Bud'ko, and P. C. Canfield, Phys. Rev. B **80**, 104403 (2009).
[23] V. W. Burnett, D. Yazici, B. D. White, N. R. Dilley, A. J. Friedman, B. Brandom, and M. B. Maple, J. Solid State Chem. **215**, 114 (2014).
[24] J. R. L. Mardegan, S. Francoual, G. Fabbris, L. S. I. Veiga, J. Strempfer, D. Haskel, R. A. Ribeiro, M. A. Avila, and C. Giles, Phys. Rev. B **93**, 024421 (2016).
[25] I. Tamura, Y. Isikawa, T. Mizushima, and S. Miyamoto, J. Phys. Soc. Jpn. **82**, 114703 (2013).
[26] E. N. Kaufmann and R. J. Vianden, Rev. Mod. Phys. **51**, 161 (1979).
[27] C. Rettori, H. M. Kim, E. P. Chock, and D. Davidov, Phys. Rev. B **10**, 1826 (1974).
[28] D. Davidov, K. Maki, R. Orbach, C. Rettori, and E. P. Chock, Solid State Commun. **12**, 621 (1973).
[29] M. Cabrera-Baez, A. Naranjo-Uribe, J. M. Osorio-Guillén, C. Rettori, and M. A. Avila, Phys. Rev. B **92**, 214414 (2015).
[30] A. Narath, Phys. Rev. **163**, 232 (1967).
[31] R. W. Shaw and W. W. Warren, Phys. Rev. B **3**, 1562 (1971).
[32] J. G. S. Duque, E. M. Bittar, C. Adriano, C. Giles, L. M. Holanda, R. Lora-Serrano, P. G. Pagliuso, C. Rettori, C. A. Perez, R. Hu, C. Petrovic, S. Maquilon, Z. Fisk, D. L. Huber, and S. B. Oseroff, Phys. Rev. B **79**, 035122 (2009).
[33] M. Cabrera-Baez, M. A. Avila, and C. Rettori, Phys. Rev. B **98**, 165106 (2018).
[34] J. M. D. Coey, *Magnetism and Magnetic Materials* (Cambridge University Press, Cambridge, UK, 2009).